Enhanced microwave transmission through a single subwavelength aperture surrounded by radial grooves

Matthew J. Lockyear, Alastair P. Hibbins and J. Roy Sambles
School of Physics, University of Exeter, Exeter EX4 4QL, UK

Christopher R. Lawrence
QinetiQ Ltd., Cody Technology Park, Ively Road, Farnborough GU14 0LX, UK

PACS: 73.20.Mf, 42.79.Dj, 84.40.–x, 41.20.Jb

Excitation of bound surface waves on textured metallic structures can lead to strong resonant absorption of incident radiation at frequencies determined by the surface profile. In the present study however, attention is turned to the role of the surface structure in the enhancement of transmission through circular, subwavelength-diameter apertures. Undertaking the experiment at microwave wavelengths allows for a precision of manufacture and optimisation of the surface structure that would be difficult to replicate at optical frequencies, and demonstrates that transmission enhancement may be achieved with near-perfect metals. Further, the use of a finite element method computational model to study the electromagnetic response of the sample allows for the fields associated with transmission enhancement to be examined, thereby obtaining a better understanding of the role of the surface profile in the enhancement mechanism.

1. Introduction

Circular apertures of diameter $d < 1.841\lambda_0/\pi$ in an opaque metal layer are unable to support propagating waveguide modes [1]. As a result, energy may only be transferred by an evanescent tunnelling process leading to very weak transmission (which is expected to scale as $(d/\lambda_0)^4$ [2]). However, the work of *Ebbesen et al* [3] generated great interest by showing that it is possible to obtain transmission of light through subwavelength hole-arrays several orders of magnitude greater than that predicted by standard aperture theory. Although studies of the microwave transmission through perforated metal substrates have been previously discussed [4], it was Ebbesen's work that specifically highlighted the enhanced transmission phenomenon through *subwavelength* apertures. Their work initiated a number of theoretical and experimental studies at optical frequencies seeking to explain the underlying physics.

The enhanced transmission phenomenon has historically been attributed to the excitation of electromagnetic (EM) surface modes that are often referred to as surface plasmons (SPs) at optical frequencies [5-8]. These authors assume that the fields associated with a SP enhance the evanescent field within the hole. Others suggest that the transmission enhancement may be entirely explained using a multiple diffraction argument [9]. Further, it has been proposed that in the case of an array of sub-wavelength slits, the SP may actually play a *negative* role in transmission enhancement due to absorption effects on resonance [10]. However it is important to note that the physics pertaining to slits is fundamentally different to that for circular apertures, as slits support a propagating TEM mode whereas sub-wavelength circular apertures do not [1].

Ghaemi et al [7] strengthened the pro-SP enhancement argument by demonstrating SP dispersion characteristics in the enhanced transmission spectrum through an array of sub-wavelength circular holes. *Grupp et al* [11] were later able to show that the magnitude of transmission enhancement was dependant only on the metallic properties of the two in-plane surfaces within a skin depth of the surface. Good metals showed a marked increase in transmission over poor metals hence they concluded that the dependence of transmission efficiency on the optical properties of the metal-dielectric interface indicated the involvement of SP's. More recently, *Lezec et al* [12] used a similar argument to explain enhanced transmission through a single circular sub-wavelength aperture, surrounded by a "bull's eye" ring structure. They attributed the enhancement in transmission to SP's supported on the illuminated surface of the aperture arrangement since the peak transmission wavelength coincides with the periodicity of the surface profile, however their theoretical model considered only a one-dimensional slit array in a semi-infinite perfectly conducting media. In addition there was strong angular confinement of the transmitted signal through the circular aperture that was attributed to the re-radiation of light back into free space by a SP supported on the corrugated exit side of the sample. *Martin-Moreno et al* [13] had previously explained resonantly excited transmission of radiation through a thin slit centred within surface grooves with the same arguments. Recently, *Barnes et al* [14] not only showed SP polarisation characteristics in the transmittance through a sub-wavelength hole array, but also SP dispersion characteristics in the absorbance, transmittance and reflectance data. They concluded that although diffraction is central to the transmission phenomenon, the effect is dramatically enhanced when coupling conditions allow SP excitation on one or both of the in-plane surfaces.

Unlike the majority of previous studies presented in the literature, of which only a small number have been commented upon above, the experimental investigation presented here is conducted at microwave frequencies. In this regime, the skin depth of the metal (of the order of microns) is very small compared to the wavelength, and as such the substrates are often wrongly considered as perfect conductors. Corrugation of the substrate introduces a surface impedance and hence an effective dielectric function [15] thereby permitting resonant excitation of bound surface modes. However the coupling of incident radiation to such modes is inefficient due to minimal absorption compared to the degree of reradiation from the mode (the magnitude of these two loss mechanisms must be equal for optimum coupling to occur [5]). Therefore at these microwave frequencies, it is suggested that the role played by the SP in the transmission enhancement mechanism may be small, yet we will demonstrate that with the addition of suitable surface topography, a 17-fold enhancement in transmission is still attained over that observed through a 'bare' aperture.

2. Sample Optimisation and Design

Finite element method (FEM) modelling software [16] is used to predict the EM response of the system and obtain the optimum design of the groove geometry with an aperture diameter of d = 2.50 mm. To reduce the mesh size and computational time, the model is simplified by making an impedance approximation on the surface of the aluminium substrate using a conductivity of $3.8\times10^{7}\,\mathrm{S\cdot m^{-1}}$. The resonant transmission wavelength was chosen so that the peak transmission efficiency would occur in the middle of a single experimental frequency range ($50 \leq f_0 \leq 75\,\mathrm{GHz}$), corresponding to a wavelength of $\lambda_0 = 5\,\mathrm{mm}$. To allow for a sufficiently deep surface corrugation on both the illuminated and exit side of the sample, the substrate thickness (h) was chosen to be 1.50 mm. Initial computational modelling demonstrated that the attenuation of the transmitted signal through the aperture was too high for signal detection. Hence the area immediately surrounding the hole was countersunk equally from each side, effectively reducing h to zero and providing a sharp ring around the circumference of the aperture (*Figure 1*).

Figure 2a shows field enhancement in the region of the aperture for $f_0 = 60\,\text{GHz}$ as a function of groove position (measured from the centre of the aperture to the centre of the groove) for a single circular groove of depth $l = 0.45\,\text{mm}$, and width $w = 1.50\,\text{mm}$, centred about the aperture. The optimum field enhancement at is found to coincide with a groove spacing of 5 mm. In the same way, further grooves were added and individually positioned, giving maximum field enhancement when all grooves were regularly spaced with a pitch $\lambda_g = 5\,\text{mm}$. The variation of field enhancement as a function of groove depth and width was then also explored at 60 GHz. (*Figure 2b and 2c*). Simultaneous variation of the dimensions of all grooves on the illuminated side of the sample shows peak field enhancement to occur when $w = 1.50\,\text{mm}$ and $l = 0.50\,\text{mm}$. Once these optimum groove dimensions and spacing were obtained it was possible to evaluate how the field magnitude in the region of the aperture varied with the number of grooves positioned in the illuminated in-plane surface. *Figure 2d* shows that the field magnitude increases steadily as the number of concentric grooves increases. It appears that the field enhancement would continue to increase with the addition of yet more grooves but a computational limit is reached with seven grooves. Subsequent studies and analysis is however constrained to a sample with four concentric rings in order to improve convergence and reduce computation time. This is sufficient to establish all principles.

3. Experimental sample and geometry

Three samples were considered (*Figure 1*): Sample A - a single countersunk circular aperture ($d = 2.50\,\text{mm}$) with no patterning, Sample B – an identical aperture surrounded on one face only by four concentric rectangular-profile grooves (two orientations, B_1 and B_2), and Sample C - an identical aperture surrounded by four concentric rectangular-profile grooves on each face. The radii of the grooves provided a periodicity of 5.00 mm, measured from the centre of the aperture to the centre of each groove. The machined grooves have a measured depth of l = 0.55 mm and width w = 1.50 mm. Radiation of frequency $50 \le f_0 \le 75\,\text{GHz}$ is normally incident upon the sample (θ = 0º), and polarised such that the electric field vector is in the x-direction.

The structures were milled into 300 × 300 × 1.5 mm aluminium alloy sheet, the edges of which were covered with microwave absorbing material to eliminate stray signals.

A schematic of the experimental arrangement used to obtain the transmission spectra as a function of transmission angle is shown in *Figure 3*. The source horn is positioned a perpendicular distance of 0.6 m from the sample and orientated such that the incident electric vector is orientated in the *x*-direction. The sample is mounted in a wooden holder and positioned over the centre of rotation of a computer controlled turntable. A 45 × 45 mm aperture formed from microwave absorbing material is positioned between the source antenna and sample to restrict the beam to a well collimated central part. A detector horn is mounted on an arm extending from the computer controlled turntable and positioned a perpendicular distance of 0.35 m from the exit side of the sample. This arrangement allowed the angular distribution of the transmitted signal to be measured as a function of frequency and transmission angle ψ for fixed values of the incident angle θ.

4. Results and Discussion

Figure 4 shows the experimental transmission data obtained from sample B_2, (with the surface profile on the illuminated in-plane surface only) normalised to the transmission through an identical countersunk aperture with no surface topography (sample A). Also shown is the modelled EM response of the sample (solid line), which shows very good agreement. Radiation is normally incident upon the sample ($\theta = 0$) and the detector is positioned normal to the surface on the exit side ($\psi = 0$). The presence of the surface corrugation on the illuminated face of the sample results in a 17-fold enhancement in transmission over that observed experimentally via the bare countersunk aperture. Note also that the maximum enhanced transmission occurs at $\lambda_0 \sim \lambda_g$, a condition compatible with any SP-enhancement argument for normal incidence, since at microwave frequencies, $k_0 \sim k_{SP}$ [5,15,18].

In order to understand the transmission enhancement mechanism, it is useful to examine the modelled EM fields close to the sample at the frequency of resonance. *Figure 5* illustrates (a) the instantaneous E-field, and (b) the time averaged H-field magnitudes. Fields are plotted in the *xz*-plane through the centre of the aperture at a temporal phase corresponding to maximum field enhancement. It is evident that the scattering of incident radiation by the concentric grooves of the sample results in a redistribution of the EM fields such that regions of high energy density are located in the vicinity of the aperture. The E-field is shown to possess maxima located at the sharp corners of each concentric groove, with maximum enhancement (25-fold) occurring at the sharp ring formed by the countersinking of the aperture entrance. The H-field however has maxima located centrally on each peak and trough of the profile. Note also that the magnitude of both the E- and H-fields in the *x*z-plane decay as a function of distance away from the aperture. *Figure 6* illustrates the relative instantaneous magnitudes of the fields on a line in this plane at a height of z = 0.5 mm (where z = 0 is defined as being situated at the uppermost part of the surface on the illuminated side of the sample). Not only are the anti-nodes in the E- and H-fields separated by 90º of temporal phase, but they are also separated spatially by approximately 90º. Thus the surface wave in this region has standing wave character, with wavelength equal to the grating pitch. However, it is not a *true* standing wave. The energy density is clearly not uniform, and in the region immediately surrounding the aperture entrance, the spatial separation of the E- and H-fields reduce slightly. This effect is due to the profile of the countersinking, and distortion of the fields due to the concentration of charge situated on the sharp ring at the aperture entrance as well as the circular symmetry of the sample. This results in a small but finite net power flow over the in-plane surface toward the aperture and an increase in the energy density, which must exist for strong transmission to occur.

Figure 6 (*inset*) shows the time averaged E-field magnitude as a function of perpendicular distance z from the illuminated surface, at a distance of 6 mm from the aperture in the x-direction. It is clear that the E-field reduces exponentially away from the interface into the incident medium (air) suggesting that the pseudo-standing wave is associated with a bound surface mode. It is important to note here however that the surface wave supported by the structure is not radial, but is dependent on the incident polarisation. This dimensionality is evident in *Figure 7* in which the time averaged E-field magnitude is evaluated over an xy-plane at z = 0.

Taking the Huygens-Fresnel view of wave propagation, when plane wave radiation is incident on a continuous surface, each point on that surface acts as an identical coherent secondary source of wavelets that mutually interfere to form the reflected wave or waves. When the incident surface possesses a periodicity, the reflected wave fronts are perturbed by a set of spatial modes possessing Fourier components that are matched to that of the structure. If we consider the periodicity in the *x*-direction and approximate the structure as an infinite plane grating, then the ±1 diffracted orders become evanescent at 60 GHz. Hence on the *xz*-plane through the centre of the aperture, strongly resonant evanescent diffracted orders will propagate along the surface undergoing successive k_g scattering and setting up the standing wave. Following the concentric grooves around to the *y*-axis, the component of the electric vector that is co-linear with the radial wave vector reduces until the E-vector is entirely orthogonal to the radial wave vector, and tangential to the surface profile at every point. Through the centre of the aperture in this (*yz*) plane, the surface corrugation results in a variation in the local H-field due to the exclusion of the fields from the metal. Hence diffraction in this direction is plane weak.

It is important to ascertain whether the evanescent fields forming the pseudo-standing wave are further enhanced by the resonant excitation of a SP. The modelling of the double sided aperture is therefore reproduced with the aluminium alloy substrate being replaced first by a perfect conductor and then a perfect insulator. This allows for comparison of each with the modelled response of the structure formed from aluminium (*Figure 8*). It is clear that peak transmission occurs at a wavelength approximately equal to the grating pitch for all three substrates. In the case of the perfect insulator, the excitation of a SP is prohibited due to the absence of free charge density at the air-insulator interface. However diffraction may still occur. Thus the increase in transmission is entirely due to the establishment of a pseudo-standing wave via near field diffraction, the fields of which are in no way enhanced by SP excitation. For the perfectly conducting substrate however, we note a 16% increase in transmission over that observed for the perfectly insulating sample. This is attributed to the introduction of surface charge and increased electric field intensity resulting from the change in boundary conditions. Due to the exclusion of the fields from the metal, it is generally assumed that a perfectly conducting structure will not support SP modes. Indeed, for a flat, perfectly conducting surface, bound surface waves do not exist. However, the presence of a corrugation at such an interface introduces effective surface impedance, which results in a bound surface state. This bound surface state is a SP, possessing a dispersion of the plasmon form, but which is characterised by an *effective* dielectric function [15].

The transmission for the aluminium alloy substrate shows a further 8% increase over that of the perfect conductor. In the microwave regime absorption of energy via Joule heating of the metal is low, but non zero. Coupling strength to the SP is governed by the balance of radiative and non-radiative (absorption) loss channels available, with optimum coupling occurring when the two are equal [5]. For the perfect conductor, absorption is zero, and hence any perturbation from this ideal system will improve coupling to the plasmon mode. As a result the fields of the pseudo-standing wave on the aluminium substrate are enhanced, thereby enhancing the fields within the aperture and increasing transmission. So, to summarise, a pseudo-standing wave is formed, resulting in a redistribution of energy density such that regions of high energy density are located in the vicinity of the aperture. As the substrate is metallic, SP enhancement of the evanescent fields may occur for real metals, but accounts for less than a quarter of the overall enhancement in transmission in the present study.

In order to investigate the angular distribution of the transmitted signals, the detector is mounted on a computer controlled turntable sweeping in the *xz*-plane. This allows the transmission spectra to be recorded as a function of frequency and transmission angle, ψ. *Figure 9* shows the un-normalised ψ-dependent transmission response on resonance of samples A, B_1, B_2 and C at the resonant frequency. As expected, sample B_2 (grooves on illuminated face only) shows a substantial increase in transmission over that recorded for the aperture with no corrugation (A). Further the corrugation on the exit face of the substrate clearly results in strong angular confinement of the transmitted signal in the forward direction. It is important to note here that although the results suggest that the sample B_1 transmits more than sample A, FEM modelling of the absolute transmission normalized to the area of the hole (not shown) suggests that in fact they are equally efficient ($T_A = 2.22$, $T_{B1} = 2.21$). The apparent increase in transmission efficiency (*Figure 9*) is because the detector horn used is only able to detect radiation which enters close to normal to its front face. Further, diffraction of the beam occurs not only in the *xz*-plane, but in all directions over a wide range of angles as one would expect for a circular hole (*Figure 10*). Comparison of the angular distribution of the transmitted signal from sample B_2 with that of sample C (*Figure 10*) illustrates the remarkable angular confinement that may be achieved with the addition of grooves on the exit face of the substrate. While the former exhibits a transmission peak at resonance possessing a width of 74º in the *xz*-plane, that of sample

C exhibits a width of only 18º. Thus it is clear that while the concentric ring surface structure on the illuminated surface simply enhances the transmission efficiency of the aperture, switching the corrugation on to just the exit side of the sample results in strong angular-confinement of the transmitted beam. A concentric ring structure on both sides clearly combines the two effects.

Figure 11 shows the un-normalised angle dependent transmission spectrum of the double-sided structure (sample C) on resonance at θ = 0, 10, 20 and 30º. The ring structure on the exit side of the sample not only confines the transmitted signal to a remarkably tight angular distribution but also forces the signal to exit the aperture normal to the surface plane largely irrespective of angle of incidence. Consider *Figure 5a* once again. It illustrates that the maxima in field magnitude on the exit face of the sample occur with the same regular spacing and position relative to the surface corrugation as those in the upper half space, although reduced in magnitude. The standing wave is reproduced on the exit face of the sample and thus there exist a number of regions of locally high field enhancement that re-radiate power. It is these secondary sources in combination with the primary source (the aperture) that results in the multiple source interference responsible for the strong angular confinement and directivity of the transmitted signal. As the position and relative magnitude of these sources are constant with respect to each other as a function of incident angle, the transmitted signal is emitted normal to the surface of the sample.

5. Summary

In the present study a thorough experimental investigation into the enhanced transmission phenomenon of a sub-wavelength aperture and photonic surface arrangement has been presented. As far as we know, this is the first such experimental study conducted in the microwave regime. In addition, the FEM modelling of the geometry has provided original insight into the transmission enhancement mechanism. A 17-fold enhancement of transmission has been illustrated, together with an angular confinement of the transmitted signal. The transmission enhancement mechanism has been shown to be primarily associated with a pseudo-standing wave formed by near field diffraction on the illuminated side of the sample. Its presence results in a strong redistribution of energy density such that regions of high density are located in the vicinity of the aperture. However, while it is often wrongly assumed that metal substrates at microwave frequencies cannot support SPs, we illustrate that the contribution to the enhanced transmission from SP-coupling is significant. The angular confinement of the transmitted signal is shown to be a result of identical patterning on the exit side, supporting a standing wave which radiates from the surface as a set of coherent sources. It is the two dimensional pattern of secondary sources that results in a complex multiple source interference pattern, giving rise to strong angular confinement of the transmitted beam, and maintaining independence to the angle of incidence.

References

1. R. E. Collin, *Field Theory of Guided Waves*, 2nd Edition, Chapter 5 (IEEE, New York, 1991).
2. H. Bethe, Phys Rev. 66, 163 (1944).
3. T. W. Ebbesen, H. J. Lezec, H. F. Ghaemi, T. Thio and P. A. Wolff, Nature 391, 667-69 (1998).
4. N. A. McDonald, IEEE Trans Microwave Theory Tech, 20, 10 (1972) (and references therein).
5. H. Raether, *Surface Plasmons*, Chapter 2 (Springer-Verlag, Berlin, 1988).
6. J. R. Sambles, Nature 391, 641 (1998).
7. H. F. Ghaemi, T. Thio, D.E.Grupp, T. W. Ebbesen, and H. J. Lezec, Phys. Rev B 58, 6779 (1998).
8. E. Popov, M. Neviere, S. Enoch, and R. Reinisch, Phys. Rev B 62, 16100 (2000).
9. M. M. J. Treacy, Phys Rev. B 66, 195105, (2002).
10. Quing Cao, P. Lalanne, Phys Rev. Lett 88, 5, (2002).
11. D. E. Grupp, H. J. Lezec, T. W. Ebbesen, K. M. Pellerin, T. Thio, Appl. Phys. Lett 77, 1569 (2000).
12. H. J. Lezec, A. Degiron, E. Devaux, R. A. Linke, L. Martin-Moreno, F. J. Garcia-Vidal, T. W. Ebbesen, Science 297, 820 (2002).
13. L. Martin-Moreno, F. J. Garcia-Vidal, H. J. Lezec, A. Degiron, T. W. Ebbesen, Phys. Rev Lett 90, 167401 (2003).
14. W. L. Barnes, W. A. Murray, J. Dintinger, E. Devaux, T. W. Ebbesen, Phys Rev Lett 92, 107401 (2004).
15. D. Sievenpiper, L. Zhang, R. F. Jimenez Broas, N. G. Alexopolous, E. Yablonovitch, IEEE Trans Microwave Theory Tech, 47, 2059 (1999).
16. HFSS, Ansoft Corporation, Pittsburgh CA, U.S.A.

Figures

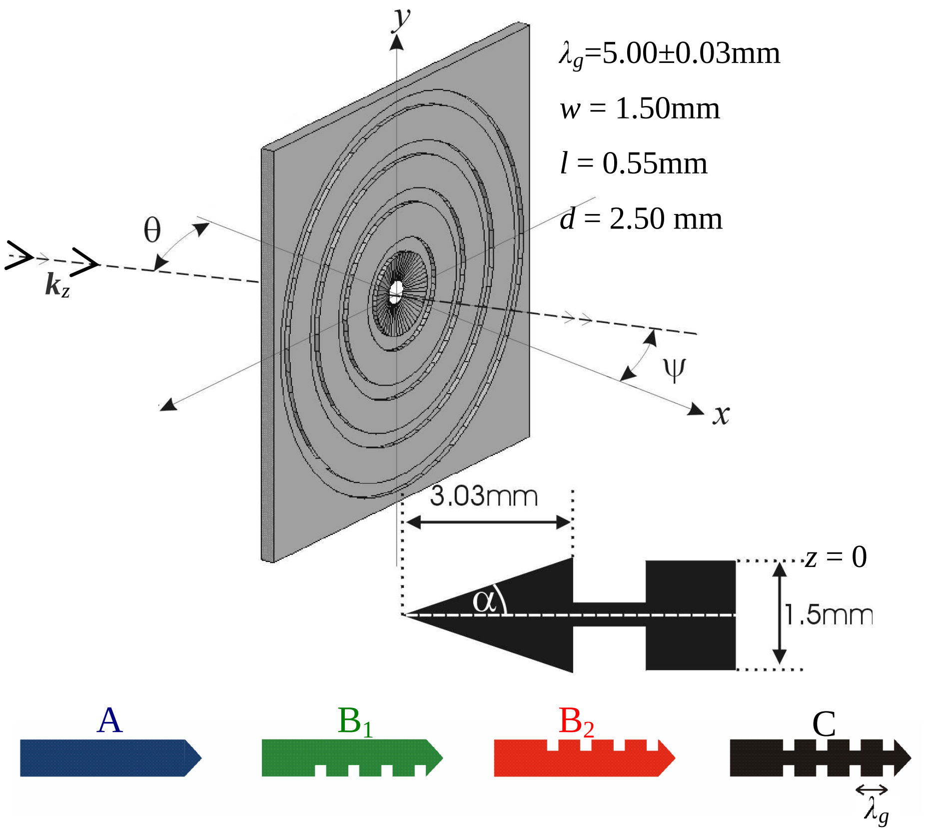

Figure 1 Sample geometry showing incident angle θ, transmission angle ψ and the countersink angle α of 13.9º. Also shown are the schematic representations of each of the three aperture geometries.

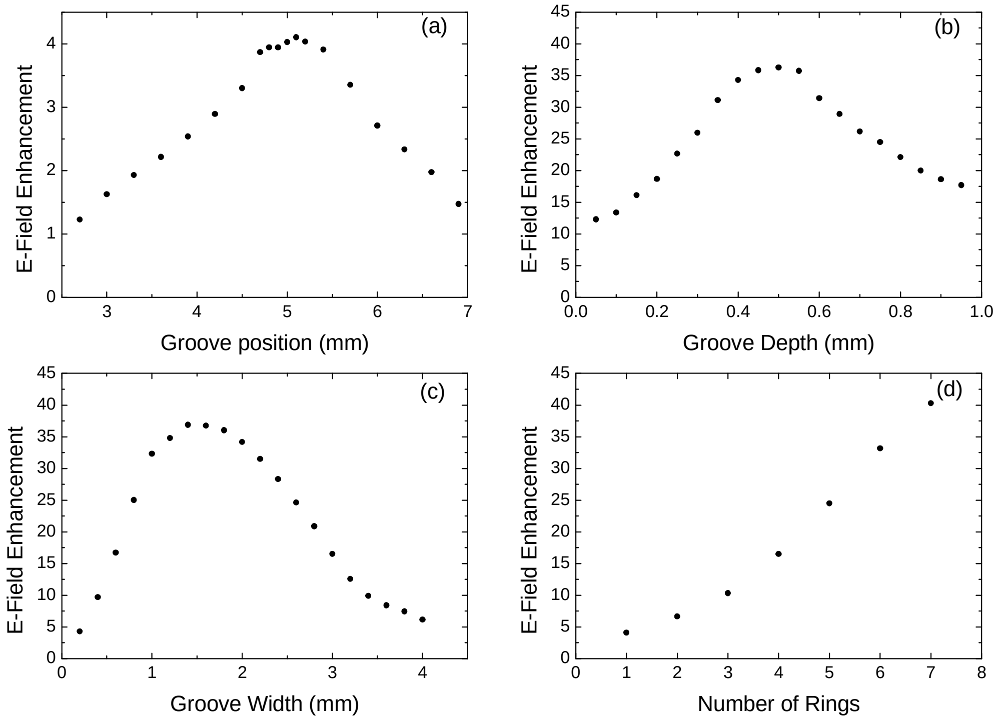

Figure 2 Computed time-averaged maximum electric field enhancement at a fixed frequency of 60 GHz as a function of: (a) groove position from the centre of the aperture to the centre of the groove for a single groove of dimensions *l* = 0.45 mm, *w* = 1.50 mm; (b) groove depth with 7 grooves each spaced by 5 mm with width *w* = 1.50 mm, (c) groove width with 7 grooves each spaced by 5 mm with depth 0.50 mm, and (d) the number of concentric rings centred about the aperture each spaced from one another by 5 mm (*l* = 0.50 mm, *w* = 1.50mm,)

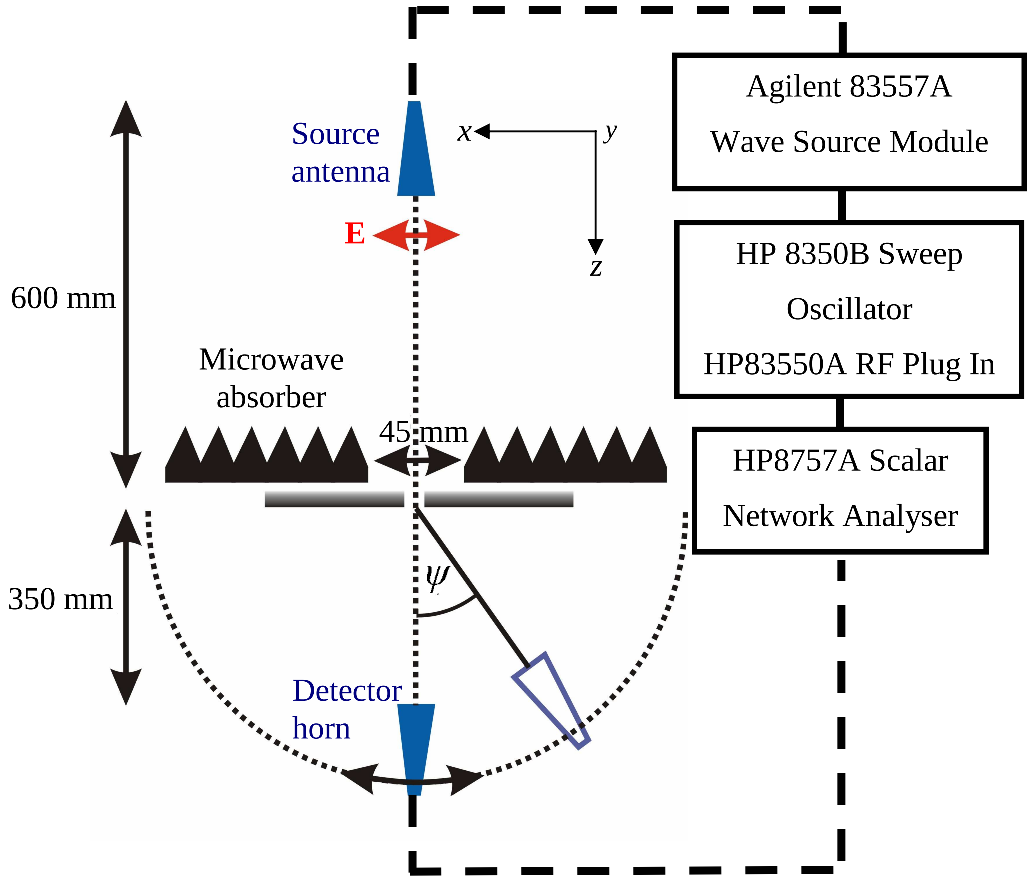

Figure 3 Experimental set up. The detector horn is mounted on an arm extending from a computer controlled turntable (*not shown*) allowing the transmitted signal to be detected over the range -70<ψ<70º.

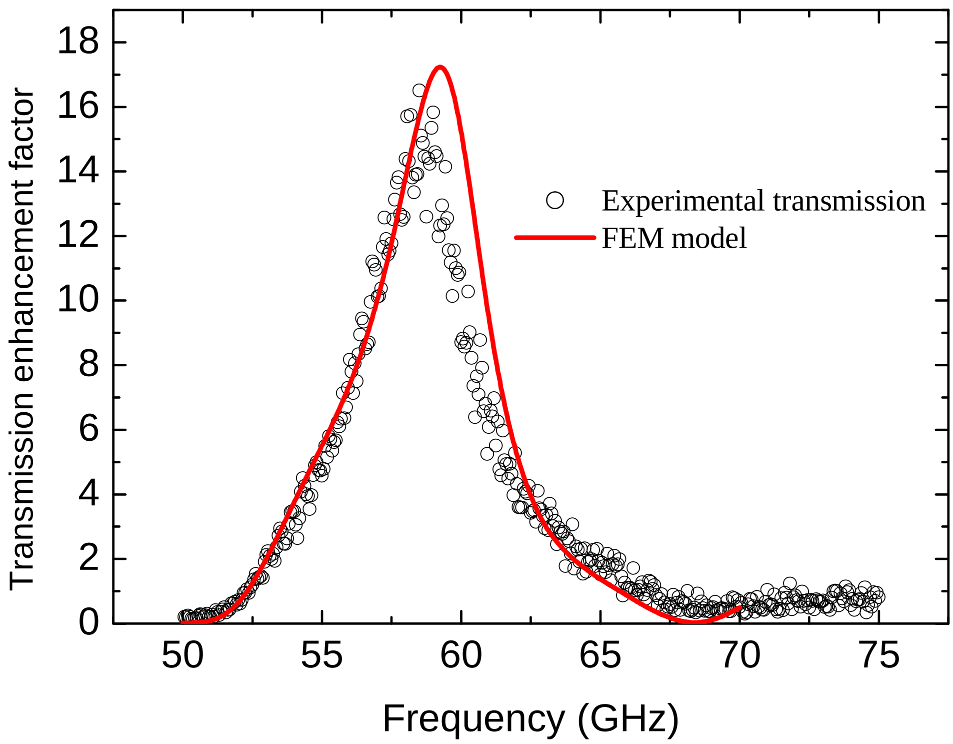

Figure 4 Transmission enhancement of the experimental double sided sample (C) normalised to the transmission of an identical aperture with no patterning. Also shown is the modelled transmission spectrum predicted by the FEM model, using the measured dimensions of the experimental sample.

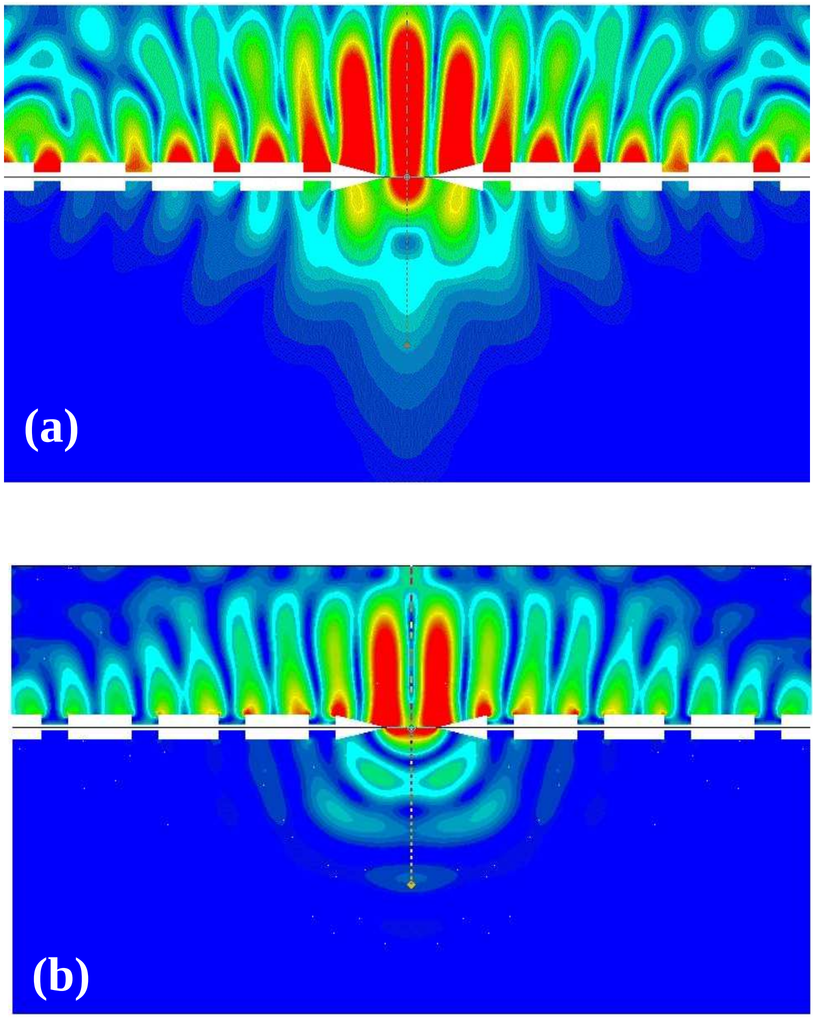

Figure 5 FEM predictions of the EM fields at the resonant frequency: (a) the time averaged magnetic field (H) magnitude, (b) the instantaneous electric field (E) strength. Both are plotted through the centre of the aperture over the *xz*-plane with the E-field at a phase corresponding to maximum enhancement.

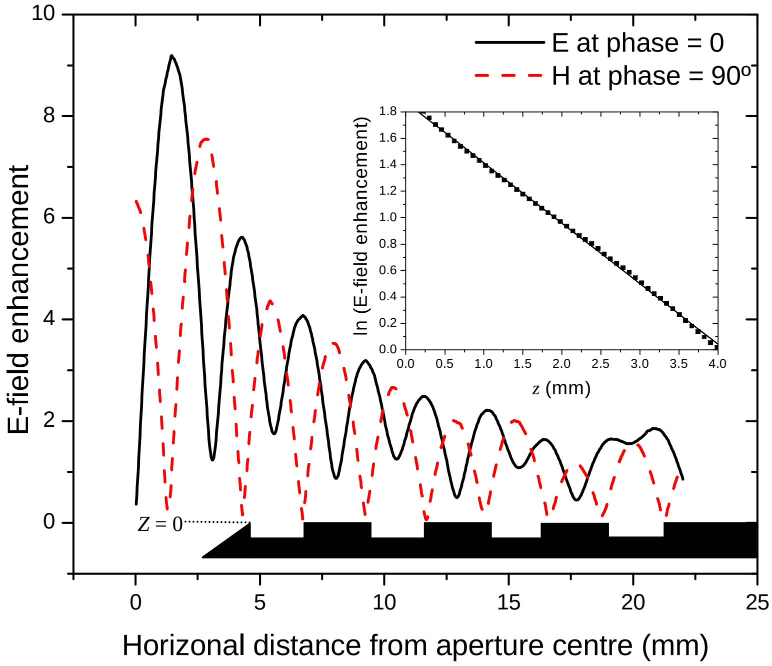

Figure 6 Relative instantaneous field magnitudes of the E (black solid line) and H (red dashed line) fields plotted over a horizontal line in the *xz*-plane. The evaluation line is situated at z = 0.5 mm and fields are obtained at a phase corresponding to maximum enhancement. **Inset:** The exponential decay of the fields of the pseudo-standing wave. The time averaged E-field magnitude has been plotted as a function of perpendicular distance z from the *xy*-plane, at a distance of 6 mm from the centre of the aperture in the *x*-direction.

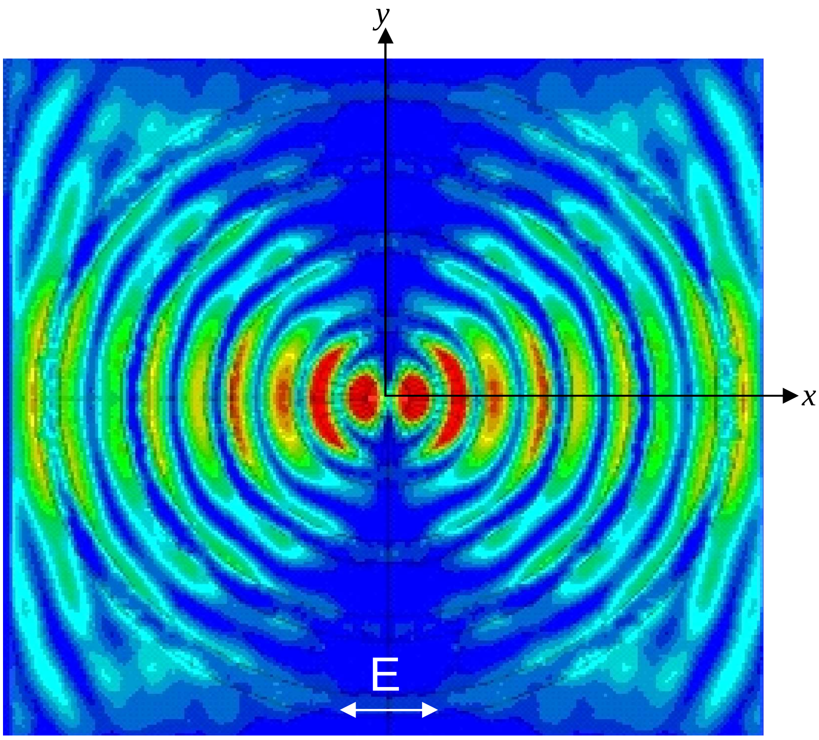

Figure 7 Modelled time-averaged E-field magnitude evaluated over the *xy*-plane at $z = 0$. Incident radiation is normally incident and polarised as shown.

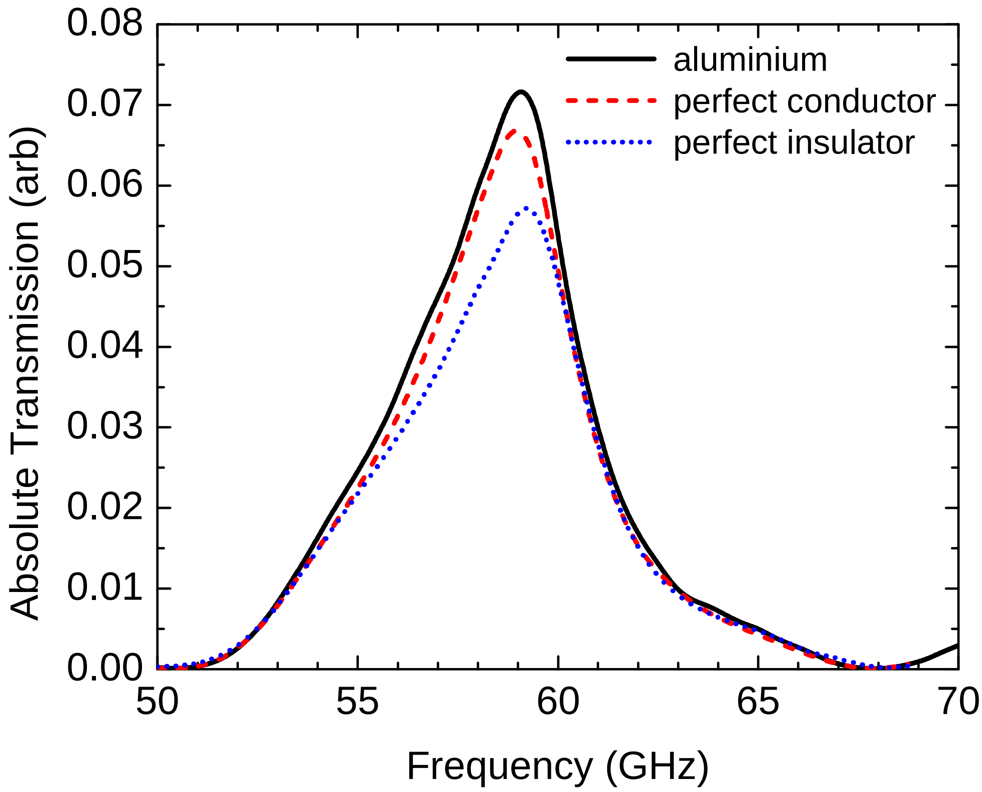

Figure 8 Modelled response of the double sided aperture describing the structure using the surface impedance approximation for aluminium (black solid line), and then as a perfect conductor (red dashed line) and perfect insulator (blue dotted line) using the measured dimensions of the experimental sample.

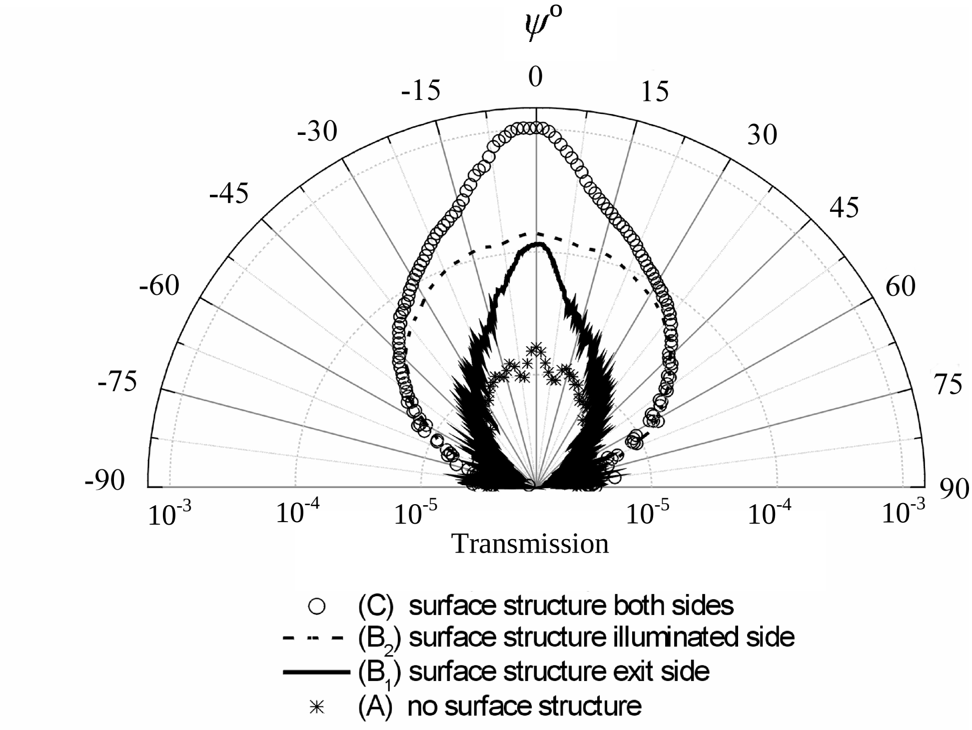

Figure 9 Experimental angle-dependent transmission spectra at the resonant frequency of each sample. (Note logarithmic scale)

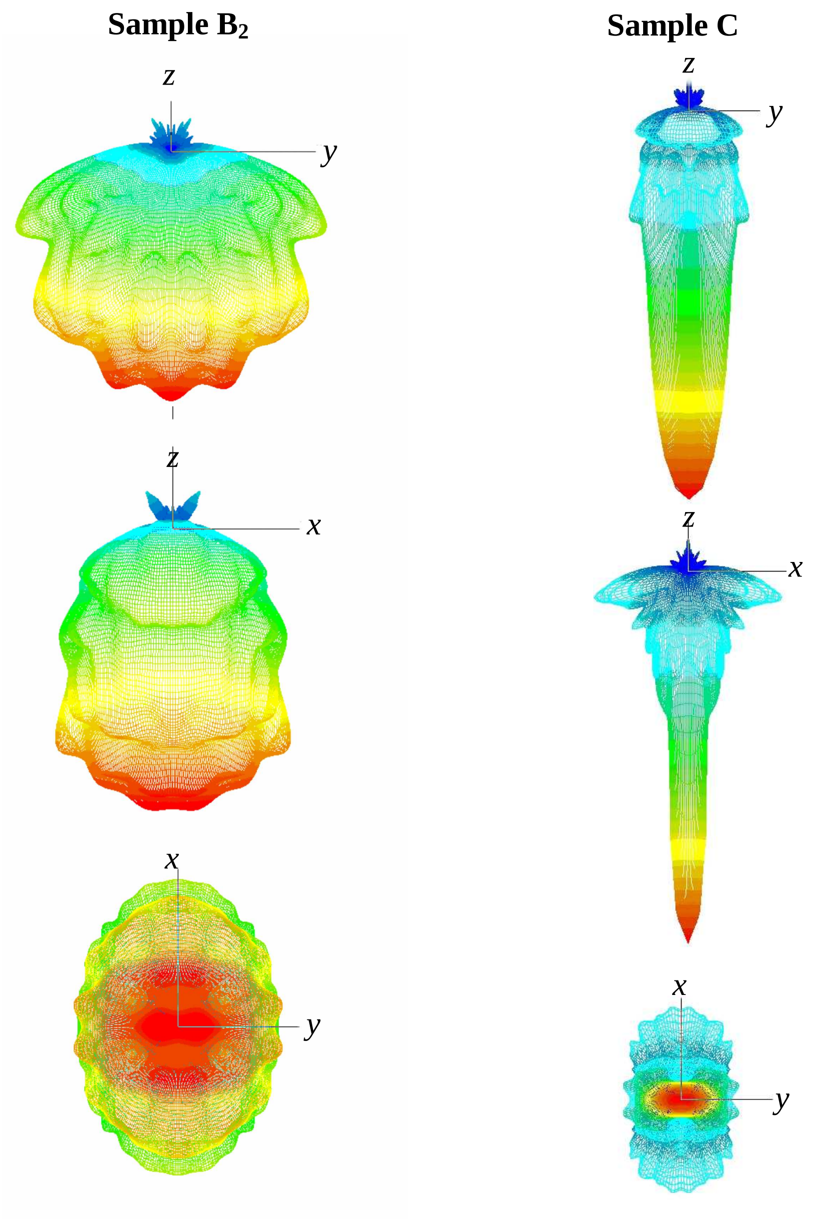

Figure 10 The modelled total radiated electric field calculated in the far field. These plots show the three dimensional angular distribution of the transmitted signal for samples B_2 (enhancement only) and C (enhancement and focusing) respectively.

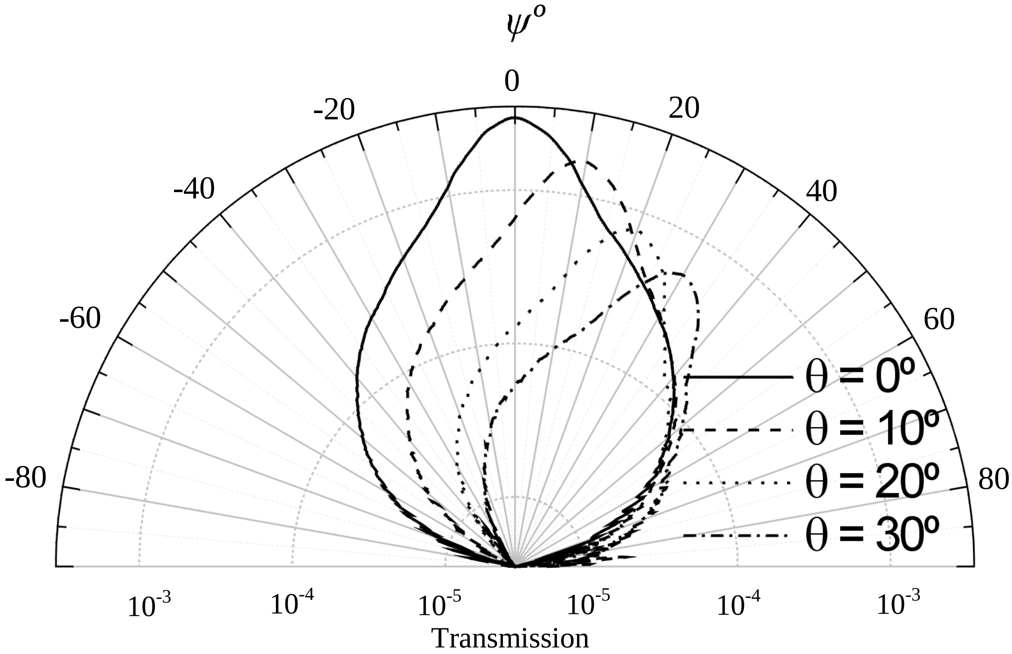

Figure 11 Experimental angle-dependent transmissivity of the structure having concentric rings on both surfaces (C), at the resonant frequency of the sample for incident angles of 0, 10, 20 and 30º. (Note for non-normal incidence the exit face of the plate is rotated by the incidence angle relative to the direction of the incident beam which defines 0° in this figure.)